Separation and Purification Technology 351 (2024) 127887

Contents lists available at ScienceDirect

Separation and Purification Technology

journal homepage: www.elsevier.com/locate/seppur

Detachment of particulate structures from a fiber array due to stretching and simultaneous gas flow

Lukas Poggemann *, Pablo Längle, Jörg Meyer, Achim Dittler

Institute of Mechanical Process Engineering and Mechanics, Straße am Forum 8, Karlsruhe, 76131, Germany

ARTICLE INFO

Keywords:
Fiber array
Clogging
Stretching
Particle structure
Detachment
Rearrangement

ABSTRACT

The main cause of high pressure drop and increased energy consumption in a filtration process is the clogging of particulate material in the upstream layers of a depth filter. To alleviate this issue, stress can be introduced into the particulate structure through stretching, which promotes rearrangement and detachment of particle structures, allowing for transfer of some of the clogged particulate material from the upstream layers to downstream void regions. This study aims to extend previous findings from experiments with single fibers to the level of an array. The goal is to analyze the introduction of a multiple stress state by performing stretching experiments with a particle-structure on a fiber array.

The stretching tests investigate the influence of different process parameters such as stretching velocity and air flow velocity during stretching on the rearrangement and detachment behavior of a separated particle structures from the fiber array. Rearrangement and detachment of the particle structure are a direct consequences of the stress induced by stretching. The experiments showed a significant increase in relative free projection area of fiber interspaces (RFPI) of up to 160% and thus a large-scale removal of particle material from the fiber interspaces when the flow velocity was increased from 0.05 m/s to 0.8 m/s. Surprisingly, the radial rearrangement of the compact particle structures during stretching resulted in a clogging and blockage of the interfiber spaces (negative RFPI in the range of minimum −54% after the first stretching cycle) and not in a total release of the interfiber spaces. The size of the particle structures in the experiments decreased by about 331 μm with the number of stretching cycles, indirectly confirming the presence of residual structures. Preliminary experiments also confirmed an increased influence on the rearrangement and detachment (removed particulater material of about 30%) of particle structures by further increasing the fiber distance of 27 μm and thus introducing a biaxial stretching into the particle structure.

1. Introduction

Depth filtration is a widely utilized technique in gas-particle technology, aiming to separate a dispersed phase from a continuous one. Its applications span various fields, including air conditioning systems and the purification of process gases. Key parameters for assessing the operation's effectiveness include separation efficiency and pressure drop. The latter signifies the energy consumption of the filtration process. As particles accumulate on top of individual filter fibers and in the void space of the fiber, the pressure drop at the filter rises. Throughout the filtration process, a gradient of deposited particle material forms over the depth of the filter with highest particle loadings on the upstream fibers [1,2]. Ultimately the filter clogs on the inlet side leaving void space without particulate material in the downstream layers of the filter. The clogging marks the transition to cake filtration with a steep increase in pressure drop [3]. When pressure drop reaches a critical point, necessitating filter replacement, it becomes evident that in-depth filtration, cleaning or re-cleaning of used filter media is not a common practice.

With the increasing demand for more energy efficient and sustainable processes, there is a growing need to reduce the consumption of filter media and energy. One possible solution to open up clogged fiber interspaces and initiate detachment of particle material within the upstream area of the filter is to apply stress to the separated particulate material. The stresses that cause the particle structures to rearrange and detach can be induced by stretching the fibers.

Experiments with a particle loaded single fiber collector have shown that stretching of the fiber can initiate the desired rearrangement and detachment of particle structures from the collector surface [4,5]. During stretching, the elongation of the substrate creates shear and tensile stresses within the particle structure, resulting in cracking of

* Corresponding author.
E-mail address: lukas.poggemann@kit.edu (L. Poggemann).

https://doi.org/10.1016/j.seppur.2024.127887
Received 23 February 2024; Received in revised form 23 April 2024; Accepted 7 May 2024
Available online 17 May 2024

the particle structure. Szabadi et al. and Zoller were able to show that the detachment of particle structures from spheriglass by magnetic deflection of a fiber or the effects of a reaction in the particle structure are possible [6,7]. In addition separate studies on the microscopic fiber surface during stretching showed that due to the change surface roughness of the fiber, the adhesion force between a individual particle and the fiber is reducing by about 33% [8].

To gain a more comprehensive understanding of the rearrangement and breakage of the particle structures within the filtration collector, the size of the model need to move from a single fiber to a fiber array. Previous investigations of rearrangement and detachment effects were limited to the observation model of a particle loaded single fiber. Single fiber stretching creates stress state within the structure. In advanced filtration processes close to the clogging point, the development of bridges between individual filter fibers within the filter are crucial for increasing pressure loss. Typically, fibers are arranged randomly or in a tangled manner, but parallel fiber arrangements occur in infinitesimal sections. For simplification and to reduce side effects, these parallel arrangements are also replicated in the fiber array (see [9]). In the fiber array, as well as throughout the entire filter medium, particles form structures between adjacent fibers. The impact of the applied process variables such as stretching velocity and flow velocity on the rearrangement and detachment of particle structures have never been under investigation at the observation level of a fiber array. The range for the applied process variables is based on previous investigations of individual fibers, as listed above. Based on the performed investigations on a single fiber, it has been determined that an air flow velocity of 0.05 m/s to 0.8 m/s is necessary to causes particle structures to break up and detach, which is promoted by fiber stretching and the applied stress. In the previous experiments with a single fiber only one-dimensional stress-state have been investigated so far [4]. In the fiber array experiments, multidimensional stress states are expected to occur within the separated particle structure due to the neighboring fibers. This idea of influencing the cracking and rearrangement of a separated particle structure has not yet been investigated. Understanding the underlying mechanisms is crucial for the effective implementation of these innovative process approaches and ideas. The knowledge of micromechanics and influencing factors can help to understand the overall process of rearrangement and detachment.

With regard to the previous investigations conducted with a single fiber, the fiber array represents a simplified form/model of an entire fibrous filter. This simplified form allows the observation of processes that normally take place within an entire filter and cannot be observed in isolation. The diameter of the fibers, the distance between them and the arrangement of the fibers have been deliberately simplified in order to enable the observation and quantification of individual processes and effects, such as rearrangement, growth and break-up of pores as well as the detachment of particle structures.

However, this simplification also involves some compromises that neglect certain effects and interactions during the loading process, but also during the stretching of the filter fibers. For example, the fibers are prototypes of a stretchable filter fiber, which is why the fiber diameter is slightly larger than the standard size. Further as previously stated, the fiber spacing is based on the published as in Müller's experiments on the separation of particles on a fiber array [9].

Another point that is different and far more complex with a complete filter than with a fiber array is the loading behavior of the filters, as well as the structural changes of the filters during the stretch. As demonstrated in a simple numerical model by Siena et al. the influence of a single (one-dimensional) layer in a random generated fiber mesh and the influence of the distribution and arrangement parameters of the fibers on the porosity and local flow velocity at and between the fibers [10]. Virtual samples were created for each porous medium, which differed in their porosity and pore-structure topology. Furthermore, specific investigations were conducted to ascertain the manner in which flow trajectories within the pores develop as a consequence of the tortuosity of the filter. Further, Alim et al. were able to demonstrate how neighboring pores develop in a porous filter medium using an analytical two-dimensional model, which was then compared to experimental data [11]. With regard to the arrangement of parallel fibers used in this study, this approach showed that with a parallel arrangement of fibers, only the presumably simplest case is considered.

Focusing on the influence of the arrangement of the filter fibers, Griffiths et al. studied the link between the tortuosity of a filter and its resulting performance. A general network model was presented to describe a filter structure comprising a random network of interconnected pores and the tortuosity of a filter and its resulting performance. It was found that the studies allow a simple scaling allows the performance curves over a wide range of the filter material properties to be mapped onto a single master curve [12]. In this context, an attempt was made to provide the deposition with a uniform framework through the parallel fibers of the fiber array.

In experimental studies using X-ray techniques, Song et al. have shown how the structure in the spaces between the fibers and the deposition of dendritic structures in the porous structure of a fibrous filter develop until clogging occurs [13]. It was found that clogging within the filter and fiber interspaces affects the particle loading characteristics of the entire filter media. The largest proportion of particles is deposited in the face regions of the filter structure (in the depth of 0–200 μm), which also affects the further deposition process. In further experimental studies, Song et al. conducted in-depth investigations into the clogging of particle structures within a filter [14]. These investigations involved the development and build-up of particle structures in the various phases of the filtration process, which were again performed using a X-ray micro-computed technique. In further studies Song et al. investigated the effects of particle bouncing and sliding on the collector during particle separation [15]. The results demonstrated that the separation of particle structures within the interspaces of the fiber changes during the entire process. Additionally, the study examines the structural alterations to the filter medium during loading. In contrast to previous studies in this overview, which employed a stiff fiber matrix, the present study utilizes a stretchable filter fiber array. This approach enables the prediction of fluid flow and permeability behavior in such a medium.

With regard to this fact, Shi et al. developed a machine learning process for predicting permeability in a deformable porous medium [16]. This process was trained on data obtained from a stretching experiment. It was demonstrated in previous studies that the permeability of the filter medium changes with stretching, depending on the orientation and previous alignment of the fibers. This is important for analyzing the processes inside the filter. The focus on a deformable and changeable medium represents a novel approach.

The starting point for the stretching experiments in this studie is always a separated particle structure consisting of polydisperse particle material on the fiber array. At the beginning of the stretching experiments, the fiber array is loaded with a particle structure in either the unclogged or clogged state. The unclogged state has unfilled fiber interspaces, allowing airflow to pass through. In contrast, the clogged state has completely filled fiber interspaces with particulate material. These loading conditions represent the filter's states before and after clogging of the upstream filter layers. The morphology of the particle structure was examined in both compact and dendritic forms, both in unclogged and clogged states. The loading conditions of the fiber array were defined based on previous investigations by Müller et al. and the investigations on the unique development of the particle structure on a stretchable fiber array [9,17,18]. Szabadi et al. and Zoller et al. have already demonstrated dendritic structures on a single fiber [6,19].

During the subsequent stretching tests, a fiber array was stretched for the first time in five stretching cycles. The stretching velocity is varied between 0.6 mm/s or 1.2 mm/s as in previous studies with the single fiber [5]. During all stretching tests the particle loaded fiber is approached by a particle-free air flow with a velocity of 0.05 m/s or

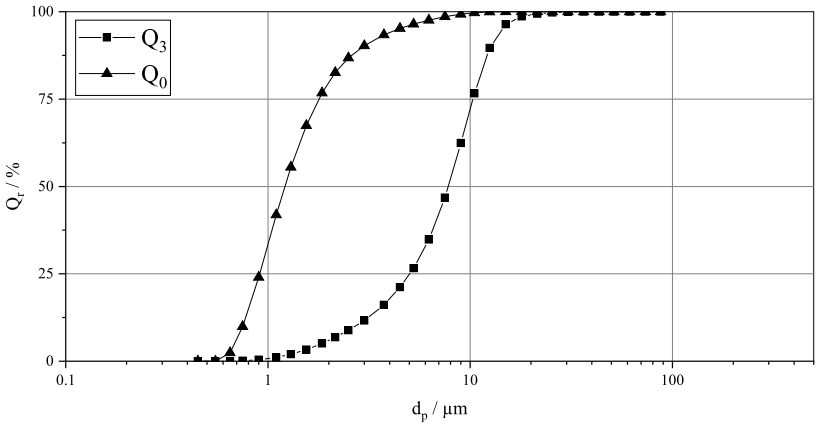

Fig. 1. Cumulative number based (Q_0) and volume based (Q_3) size distribution of the used polydisperse particulate material Spheriglass5000CP.

0.8 m/s.gate this simplified type of stress Similar to the single fiber experiments conducted by Poggemann et al. the fibers in this study were initially stretched only in the axial direction to invest its application [5]. The study recorded the size and moment of detachment during the stretching process to quantify the rearrangement and detachment of particle structures, as in previous studies. Experiments will also be conducted to obtain a qualitative understanding of the fracture process and rearrangement on the fiber array for the first time. The aim of this analysis is to complement the thorough investigation of structural modifications presented in [18]. Further, the size analysis of the detached particle structures and their moment of detachment is particle structure. To evaluate the overall effect of stretching on the amount of deposited particle material on the fiber array, the total relative particle occupancy of the array is calculated after each stretching cycle.

In addition to the stretching tests with a fixed fiber distance and axial stretching, for the first time preliminary tests with a flexible fiber distance have been investigated. In this experiments the fiber distance can be flexibly changed by at least 27 µm during the elongation process by means of a variable angle of the fiber clamping. This biaxial stretching is intended to show the change in pore size during the stretching of an overall filter. As a result a multidimensional stress state is generated in the deposited particle structure due to the elongation and simultaneous change in fiber distance. Cracks can emerge within the due to stretching of substrate as shown by Beuth et al. Natha et al. and Thouless et al. [20–23]. Theoretical considerations of stress distribution have been made by Jia et al. and Ochai et al. [24,25]. The fibers are not only stretch in the direction of the fiber axis, but also shift relative to each other in the axial direction with different deflections. The rearrangement and breakage of the particle structure on the fiber array were analyzed using only qualitative image analysis in the direction of the particle-free airflow. This study aims to investigate the influence of different process parameters, such as stretching velocity and air flow velocity during stretching, on the rearrangement and detachment behavior of particle structures from the fiber array. The rearrangement and detachment of particle structures are direct consequences of multidimensional stress induced by stretching.

2. Material and methods

2.1. Fibers and particulate material

All studies were conducted using stretchable polyurethane filter fibers that can be stretched up to 75%. The fibers have an average diameter of 82 µm and exhibit a crimped shape in their initial state. Stretching the fibers to 55% elongation results in a diameter reduction of approximately 18%. The elastic modulus of the fiber is measured at 0.49 MPa.

As in previous studies, inert polydisperse Spheriglass 5000 CP00 particles (Potters Industries LLC) was used in all experiments [5,6,19]. The particle size distribution shown in Fig. 1 was determined by light scattering analysis using Helos, Sympatec. All analyses refer to the $x_{50,3}$ = 7.82 µm of the particle size distribution. Prior to use in the loading procedure, the particulate material was dried in an oven for a minimum of 48 h to facilitate dispersion.

2.2. Stretching device

A specially designed fiber clamping device (Fig. 2(a)) is used to hold the fibers during the loading and subsequent stretching of the fiber array. The device allows the clamping of five parallel filter fibers between two opposing combs with a defined tooth spacing of 246 µm and a distance of 51.9 mm. In this respect, the clamping device is similar to the one used by Poggemann et al. to study the development of morphology [8]. As in previous studies, a desired fiber elongation of 38.5% is achieved by stretching 22 mm. In contrast to the previous study, the holder shown here has a piezoelectric motor (PI, Q521-230) under each of the two clamping blocks to allow a maximum movement of 11 mm per side. Due to the strength of the five elastic fibers, the maximum stretching velocity is limited to a maximum of 1.2 mm/s. In order to change the fiber distance during the stretching process, there is a second fiber clamping device (see Fig. 2(b)) in which the clamping of the fibers is rotatably mounted. The objective is to achieve simultaneous strain by changing the fiber spacing, creating a biaxial stretching and multidimensional stress state in the particle structure. Piezo motors are used for the linear movement of the fiber clamping device for uniaxial stretching. To enable rotation of the fiber clamp around the vertical axis, horizontal ball bearings are mounted between the motors and the fiber clamp. The clamps are affixed to the side of a model servo using a 3D-printed L-bracket (see Fig. 2(b)). The servo gearing enables various rotation angles of the attached fiber clamp. The fiber clamp's rotation and linear movement are achieved by connecting a pin in a groove. The fiber distance can be reduced or increased by up to 27 µm by rotating by up to 45 degrees. Fig. 3 shows the main principle of enlargement of fiber distance using rotation of parallel fibers. This principle has already been used in a simplified ans static form by Müller et al. Both clamping constructions are mounted on aluminum plates for easy handling [9]. Prior to each load, the fiber array is cleaned with compressed air and isopropanol. All five fibers are replaced after three experiments.

2.3. Aerosol generation and loading procedure

The aerosol, with a volume flow of 26.3 l/min (feed flow), was generated using the SAG 410/U by Topas, a system previously employed in studies by Zoller et al. Wang et al. and Papapostolou et al. [19,26,27].

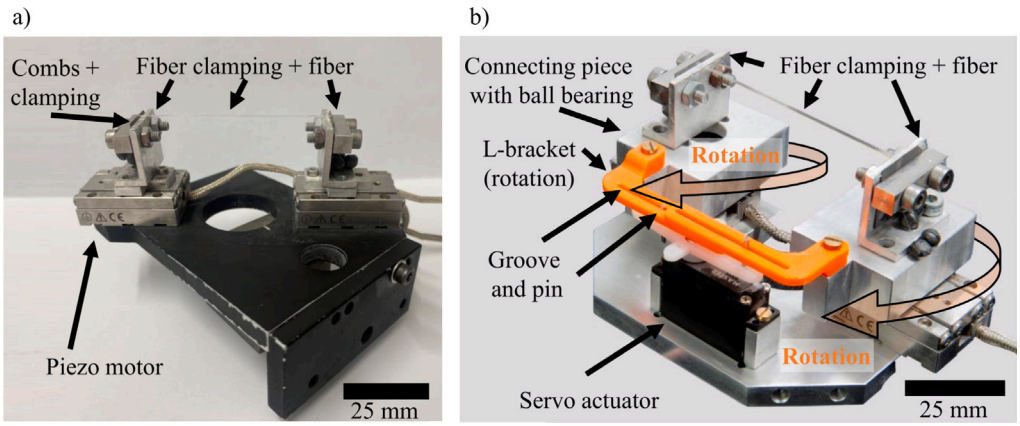

Fig. 2. (a) Clamping device for just stretching the fiber array (b) Clamping device for simultaneous stretching and changing the fiber distance by rotating the clamping combs.

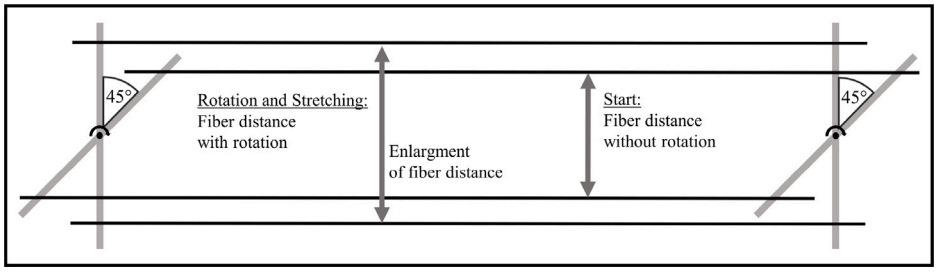

Fig. 3. Schematic representation of two clamped fibers. It is possible to enlarge and reduce the fiber distance by rotation of the fiber clamp. Here the increase in the fiber spacing.

Fig. 4 shows the Particle dispersion was achieved by sucking particulate material from a steel ring through a venturi nozzle. Additionally, the aerosol underwent neutralization using an 85Kr-neutralizer. A part of the generated aerosol was discarded after particle removal through a HEPA filter. The remaining loading flow passed through the inlet pipe equipped with a flow rectifier (diameter 16 mm) and entered the loading chamber, approaching the fiber array. The particle loading process for the array was executed within a 16 mm free jet airflow at varying flow velocities. Downstream of the fiber array, another HEPA filter was employed to remove any remaining particulate material. The mass flow was controlled using a mass flow controller (MFC). This detailed process ensured precise control and monitoring of the loading flow throughout the experiment.

Aim of the experiments is to compare different particle structure/loading conditions at different airflow velocities at the same particle concentration in the aerosol during the loading procedure.

The time integrated flux (TIF) is used to calculate the number of particles (polydisperse particle material) that have passed a defined control area over a given time interval considering the current air flow velocity. Therefore, loading was performed until a certain number of particles per cross section had flowed towards the array. The basic considerations for this form of particle and particle count detection are based on the investigations of Raasch et al. [28]. First, the particle flux density (j_i) is calculated using the particle concentration c_p of the aerosol and its velocity u (see Eq. (1)).

$$j_i = c_p \cdot u \tag{1}$$

The TIF in $\text{particles per mm}^2$ can be obtained by combining the particle flux density j_i with the respective loading time t for a specific time interval.

$$TIF = J(t) = \int_0^t j_i \, dt \tag{2}$$

$$TIF = J(t) = t \cdot j_i \tag{3}$$

For a constant j_i:

$$TIF = c_p \cdot u \cdot t \tag{4}$$

In earlier studies by Poggemann et al. the progression and clogging of the fiber interspaces of the array by particles was investigated in detail [8]. This process, also known as clogging, is of great interest as it marks the start of the transition phase and the increase in the pressure loss curve of a filtration process. It divides the usual filtration process of depth filtration into a first section in which further aerosol can still flow through the fiber inerspaces. In the second stage of the advanced filtration process, the spaces between the fibers are blocked by particle material. The particle structures on the individual fibers grown together to form a clogged structure. This is followed by a steep increase in pressure drop due to the formation of a layer of dust inside the filter and on the surface of the upstream side.

In order to adequately characterize the rearrangement and detachment behavior of particle structures, it is necessary to study different types of particle structures. Therefore, the morphology of the particle structure on the array is varied. Either dendritic or compact structures are deposited on the fiber array, depending on the Stokes number. For each of these structures of different morphology (compact and dendritic), a distinction is then made between a non-clogged and a clogged structure depending on the TIF. The corresponding deposition parameters for all states are listed in Table 1.

2.4. Stretching procedure

All uniaxial stretching experiments without changing the fiber distance are performed with a non-clogged and a clogged particle structure on the fiber array. In addition, a further set of experiments was performed on the fiber array blocked by a particle structure in which the fiber distance is reduced or increased by 27 μm. In the present investigation, a sequence of five consecutive stretching cycles was

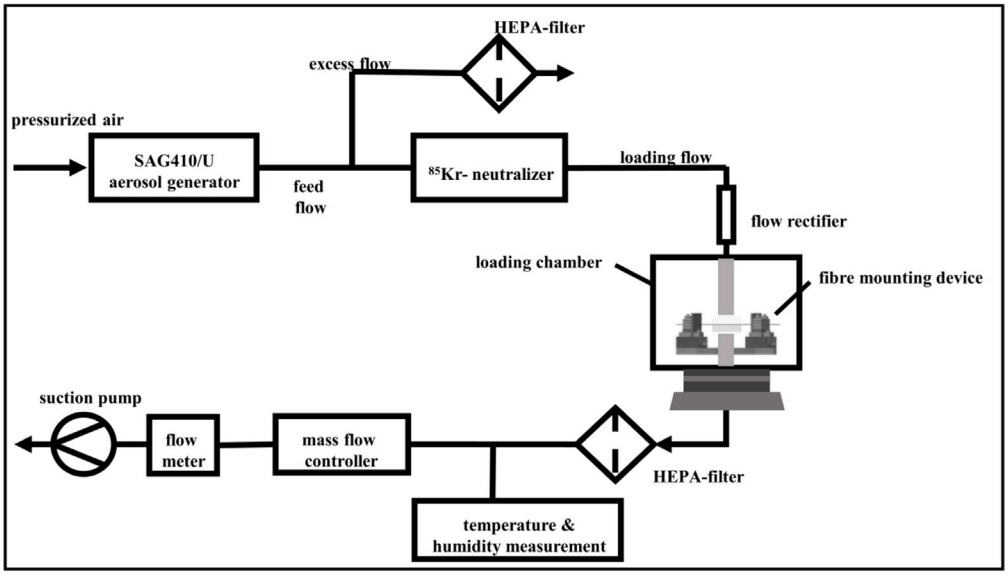

Fig. 4. Schematic setup to produce an aerosol containing glass spheres and the deposition on an fiber array that is clamped at the fiber mounting device [5].

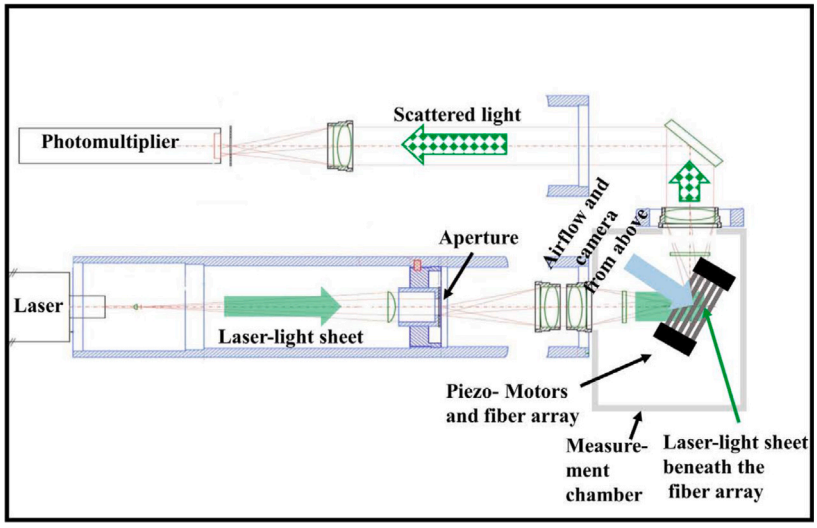

Fig. 5. Schematic diagram of the laser thin film measurement system. An expanded laser beam (thin sheet) passes beneath the fiber array. The scattered light within the measurement area is focused onto a photomultiplier and converted into electrical pulses.

Table 1
Dimensionless numbers of the loading procedure.

Flow velocity m/s	Volume rate L/min	Re –	St –	Pe –	TIF 10^8# mm^{-2} (non-clogged structure)	TIF 10^8# mm^{-2} (clogged structure)	Morphology
0.146	1.76	0.78	0.82	3.9	1.73	4.06	dendritic
0.65	7.84	3.48	3.62	17.3	1.73	4.06	dendritic
1.2	14.48	6.42	6.70	32	1.73	4.37	compact
1.8	21.78	9.64	10.05	47.9	1.73	6.05	compact

Table 2
Parameters for the stretching process. All parameters were combined and applied in each range of particle structure morphology. Experiments are performed, both with and without changing the fiber distance.

stretching velocity/ mm s^{-2}	air flow velocity/ m s^{-1}	stretching length/ mm	change of fiber distance/ µm
0.6; 1.2	0.05; 0.8	22	0; ±27

performed. Elongation velocity and airflow velocity remained constant throughout the stretching and relaxation process of the fiber. All experimental procedures were performed in triplicate. Throughout the stretching cycle, a particle free airflow was directed towards the fiber. Table 2 summarizes the experimental parameters for the stretching experiments. The unblocked area within/in the fiber interspaces was analyzed at the end of each stretching cycle using image analysis techniques as described in Section 2.6. The size of particle structure fragments are measured with the Large Structure Detection System (LSDS) (quasi in situ) during each stretching cycle.

2.5. Experimental setup for size characterization

For the measurement of the scattered light equivalent size of the detached particle structures, the specially constructed laser light measurement technique is available [5,29–31] (see Fig. 5). In the setup of the measurement technique, a laser with the wavelength 532 nm is expanded to a 16 mm wide and 2 mm high laser-light sheet. During

stretching a particle-free airflow is approaching the fiber array. Further a camera is used in direction of airflow to determine the RFPI. When the detached structures from the array pass the laser band, light is scattered accordingly and converted into an electrical signal using a photomultiplier. The assignment of the signal height to the corresponding scattered light equivalent size of the particle structures is done by a previously performed calibration with glass spheres. For the measurement of structures detached consecutively from a fiber array in rapid succession, the measurement technique was improved with respect to the counting rate and the identification of superimposed signals using software. By analytically approximating the acquired signal structure, superimposed signals from two particle structures following each other quickly can be identified and considered individually. This case was expected for a fiber array with a significantly larger amount of deposited particle material. The measurement range of the laser light measurement technique is from 90 µm to 2000 µm. The sampling interval is $1 \cdot 10^{6}$ s, which means that even structures deposited in rapid succession can be detected with a minimal signal length of around $1 \cdot 10^{-4}$ s.

2.6. Determination of relative projection area of free space in the fiber interspaces

To capture the rearrangement and detachment of the particle structure on the fiber array during the stretching process, a Basler camera acA4024 29uc for video recording is used in direction of airflow. The camera has a resolution of 4024 × 3036 pixels and a variable frame rate up to 31 fps in full resolution.

By using a camera system mounted in the direction of flow, it is possible to observe the stretching process and thus quantify the rearrangement of the particle structure on the fiber and in the inner interspaces of the fiber by image analysis. The perspective is the same as in the array loading studies [8]. The illumination takes place via red ring light, which illuminates in the direction of flow. To quantify the fractured structure and the free flow area within the particle-loaded array, the relative free projection area in the interspaces of the fiber is calculated. The calculation of RFPI can be found in Eq. (5).

$$RFPI = \frac{1 - A_{particle,i}}{A_{particle,0}} = \frac{1 - A_{total} - A_{pore,i}}{A_{total} - A_{pore,0}} = \frac{A_{pore,i} - A_{pore,0}}{A_{total} - A_{pore,0}} \quad (5)$$

Herein A_{total} denotes the overall area of the fiber array interspaces in the non-loaded stage, $A_{pore,0}$ is the area of pores at the beginning of the stretching process (after the loading process) and $A_{pore,i}$ the area of pores after the i-te stretching cycle. Fig. 6 further shows the processing steps from the preparation of the projection images to the calculation of the cleaning efficiency or the RFPI in the inner fiber interspaces in a flow chart. The image section at the time directly after loading can be seen at the top, whereby the fiber environment was removed with a Matlab routine. The correct section of the image was cropped, rotated and binarized. As shown in the second image from the top in Fig. 6 the particulate material is colored white. In the next step/image the image was inverted in order to be able to analyze the unoccupied area within the fiber interspaces. In the third image, the white area then represents the unblocked area in the particle-loaded fiber array A_{pores}. The size of this area is determined by counting the pixels. The fourth image from the top Fig. 6 shows the same section of the fiber array after 5 stretching cycles. The processing steps cropping, binarizing and inverting have already been carried out. The fiber environment was also hidden using the Matlab routine. During the 5 stretching cycle, particle material was clearly detached from the fiber array, which increased the unblocked regions on the fiber array ($A_{pore,5}$). This can be seen as the white area in the cropped image. The RFPI provides insight into the changes that occur within the fiber array interspaces after each stretching cycle in the initial load. The following interpretations can be made:

- $RFPI > 0$: release of clogged inner pores (complete release if RFPI = 1)

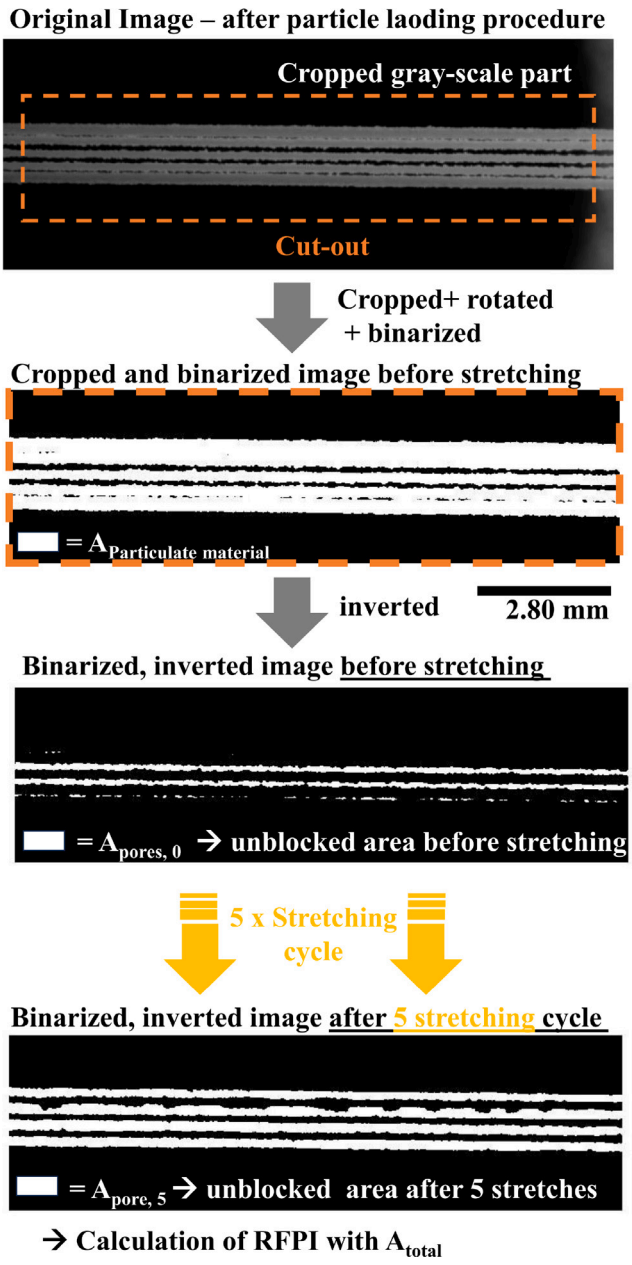

Fig. 6. Schematic procedure for determining the proportion of unblocked area in the fiber interspaces of the array.

- $RFPI = 0$: No changes in the free inner pores
- $RFPI < 0$: Clogging of the inner interspaces of fiber array due to rearrangement

The evaluation process involves the usage of a custom-developed MATLAB routine which is given in the Support Information (SI). The application of tensile forces to the fibers in the experiment did not result in any significant alterations to the measured RFPI values for the fiber array. To illustrate this, five consecutive strains were performed without the addition of particle material. There were no significant changes in the projection area. The corresponding images of the experiments can be viewed in the SI.

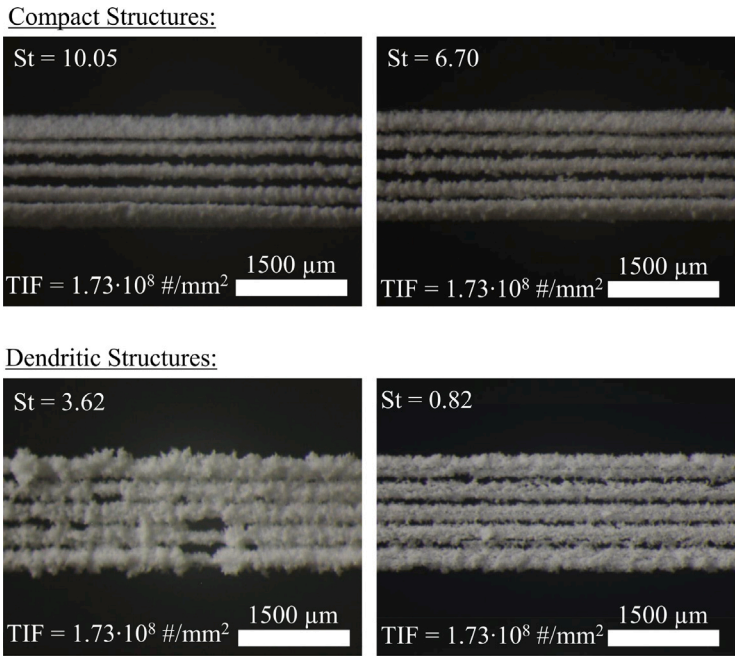

Fig. 7. Morphology of the non-clogged particle structures on the fiber array as a function of the Stokes number.

3. Results and discussion

3.1. Morphology of particulate structure on the fiber array before clogging

Fig. 7 depicts macroscopic images of the generated particle structure with non-clogged fiber interspaces (TIF = 1.73 $\cdot 10^8$ # mm^{-2}). The structures on the fiber are not yet fully clogged or grown together and represent the non-clogged structures which are used for the first set of stretching experiment.

The morphology of the non-clogged particle structures on the fiber array is a function of the Stokes number. All structures shown here were taken from the particle loading process of the TIF listed in Table 1. The preliminary investigations on the development of the structures on the fiber array for high stokes numbers can be found in the studies by Poggemann et al. [8]. Compact structures (Fig. 7, TOP) show minimal particle bridging, which leads to large horizontal pores between the fibers. These compact structures tend to form at the stagnation point of the fiber.

In contrast, irregular dendritic structures (Fig. 7, BOTTOM) show increased bridging due to their increased contribution to diffusive deposition, which leads to the formation of numerous small interspaces between the fibers. The particle structures show an increased number of small dendritic branches growing into the fiber interspaces as observed in the investigation by Szabadi et al. [32]. In addition, a increased porosity of the particle structure is clearly recognizable.

3.2. Detachment of particle structures from a fiber array before clogging

3.2.1. Development of structures during uniaxial stretching

Compact and dendritic structures exhibit distinct differences in their detachment behavior during stretching. For a compact structures, the detachment process from the fiber array can be divided into three steps. These steps are illustrated in Fig. 8 on the left. In the first phase, the compact particle structure moves in sync with the fiber experiencing elongation, without any formation of cracks. The deposited particle structure remains attached. During this phase, the adhesive forces between particles dominate over the forces induced by fiber stretching. This prevents the formation of cracks within the particle structure.

Usually at one-third of the desired fiber elongation, cracks begin to develop within the particle structure, although no particle agglomerates have yet separated from the structure. From the camera perspective in this investigation, it is not entirely clear where the crack occurs within the particle structure. However, since the individual particle structures on the neighboring fibers of the array are still without any real connections, it cannot be assumed that the cracks of the parallel structures are influencing each other. However, the structure is slightly loosened from the fiber surface and individual particles are rearranged.

The second phase is marked by the growing of cracks. As the fiber stretching continues, the cracks expand and generate multiple small particle structures on the fiber. Due to the lack of contact to neighboring structures, these small particle agglomerates have significantly less stability than the initially formed particle structure before stretching. As stretching proceeds, the small particle structures start to rearrange in radial direction gradually with each fiber of the array. The particle structures can move into the interspaces of the fiber array (not shown here for the sake of clarity). Regardless of the direction of radial rearrangement, and regardless of whether the structures move into the fiber interspaces, this results in an increase in the face area of the particle structure. This leads to an increase in stress due to flow forces. In addition, the angle of attack of the external force caused by the flow changes. The movement of particle structure is mainly due to the stretching of the fiber which might induce a slight rotation of the fiber that is finally transferred to the particle structure that rearrange in radial direction in the following. The third phase of the stretching process starts with the detachment of the first particle structures.

The detachment behavior of dendritic structures can also be divided into three phases, similar to compact structures. Due to the increased contribution of diffusive deposition mechanisms, dendritic structures tend to deposit uniformly on the flow-facing side of the fiber while the compact structures at high stokes numbers grow mostly towards the upstream direction in a narrow range around the stagnation point. In addition, the typical small dendritic branches are formed on the sides of each fiber and are thus automatically perpendicular to the air flow during stretching procedure.

In the case of dendritic particle structure on the array, the stretching process starts in phase 1 with the movement of the particle structure with the stretched fiber.

In the following cracks are formed within the particle structure (phase 2). However, the resulting cracks do not emerge throughout the

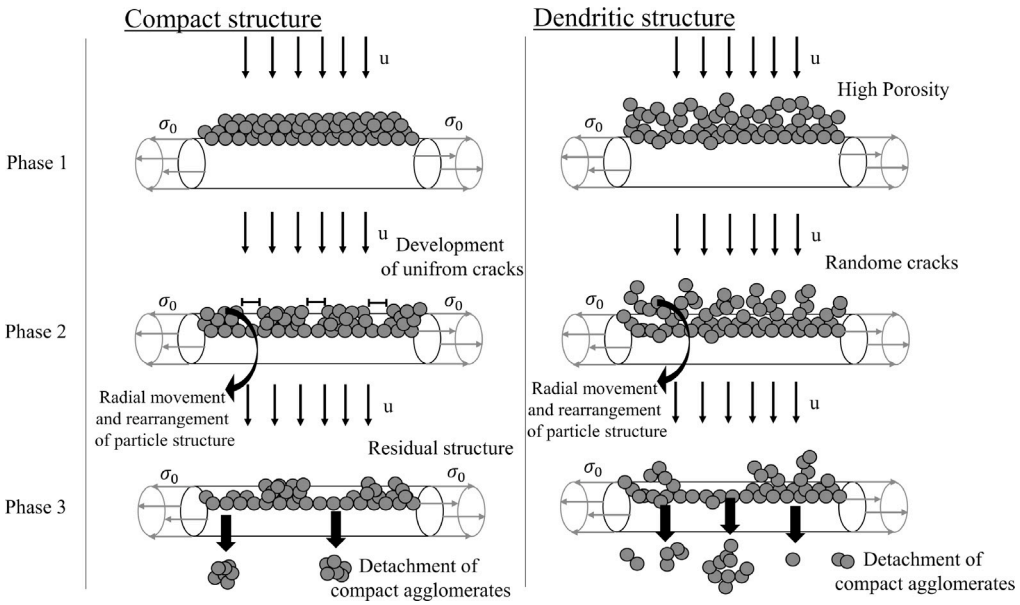

Fig. 8. Schematic of the three phases of detachment. Left: compact structures, Right: dendritic structures. Crack building, radial rearrangement of particle structures and detachment are visible.

entire particle structure as they just occur more local due to higher porosity of the particle structure. In addition, particle structure start to move slightly perpendicular to the fiber axis. This radial rearrangement of the structures is not nearly as pronounced as with the compact structures. Presumably, there is also a difference in the overall adhesion between the fiber and the particle structure, which can also be explained by the lower porosity and fewer contact points.

With further fiber stretching, only the outermost dendrites of the particle structure detach, which marks the start of phase 3. After the first detachment of the dendrites, larger structures start to detach and peel off from each fiber.

In all experiments with compact and dendritic particle structure, a residual structure remains on the fiber surface after detachment of particle structures during stretching. This indicates disruption of particle-to-particle bonds rather than particle-to-fiber bonds.

If there are remaining particle material on the fiber after the stretching, during relaxation of the fiber the individual structures may move radial back to the position before stretching. The cracks within the dendritic structures are clogged if there are locally neighboring particle structures on the fiber. In the case of compact structures small agglomerates may do not detach during the stretching, compact structures can remain suspended in the spaces between the fibers and are slightly compressed due to the relaxation of the fiber. Further they move in radial direction during the relaxation process. If particle structure remain in the fiber interspace they are partially supported by the neighboring fibers. Though the cracks are mostly closed, but the changed surface structure clearly shows that a rearrangement has taken place.

In experiments with compact and dendritic structures, the previously formed cracks are closed during relaxation, and during subsequent stretching, the structure tends to fracture again preferentially at the same locations as before. Considering the number of detached agglomerates, significantly fewer particle agglomerates separate during relaxation than during stretching. Therefore, the following analysis focuses only on the agglomerates detached during stretching.

3.2.2. Development of moment of detachment during uniaxial stretching

In the following plots, the moment of detachment of particle structures refers to the corresponding elongation of the fiber at the moment of detachment during the elongation process. A plot over elongation was chosen for this plots because it is independent of the elongation rate of the fiber during the stretching process. The same form of illustration was chosen in the previous publication for the detachment of particle structures from a single fiber [5]. From the data, patterns can be extracted that provide information on how often and at what elongation the collector must be stretched to detach particle structures. In addition to the morphology described above, the stretching speed and the air flow velocity are varied in experiments.

The graphic in Fig. 9 plot the size of the released particle structure over the fiber elongation at the moment of detachment for each detachment event. Detachment events during the first stretching cycle are represented by solid symbols, while events in the 2.-5. cycle are consolidated marked by outlined symbols. Delayed release of particle structures after the end of fiber stretching may result in the detection of particle structures beyond the intended and advertised range of fiber elongation. These particle structures were assigned an elongation of 38.5% (maximum elongation) in the application.

Regardless of the morphology (St = 3.62; St = 10.05) of the particle structure on the fiber and the stretching velocity, during the first cycle almost no particle detach in the first 25% of stretching at low airflow velocities of 0.05 m/s. It is assumed that the force of the airflow is not strong enough to detach the particle structure from the fiber in individual agglomerates. In all experiments regardless the morphology (St = 3.62; St = 10.05) the most frequent area for detachment is the area of 20–38.5% of stretching which is independent from the corresponding stretching cycle. Looking at all experiments with high air velocity (0.8 m/s), there is a first detachment of particle structures at stretching of 5–10%. The detached particle structure in the 0.8 m/s experiments (St = 3.62; St = 10.05) is on average larger than the structures detached within the experiments

In the second to fifth stretching cycle some particle structure detach at less than 5% of stretching. This observation is independent of the morphology of the particle structure on the fiber. The successive stretching causes a loosening of the deposited particle structure due to induced cracking, which also leads to detachment at lower flow velocities.

In the experiments with low stretching velocities the majority of particle structures detaches in the 2.–5. cycle. In the experiments with a high stretching velocity of 1.2 mm/s most particle structures detach at the end of the first stretching cycle in the range of 25–28% of fiber stretching. For a possible application in filtration, this means that the collector only needs to be stretched slightly faster in order to achieve improved particle detachment at the end of the first cycle, but the flow

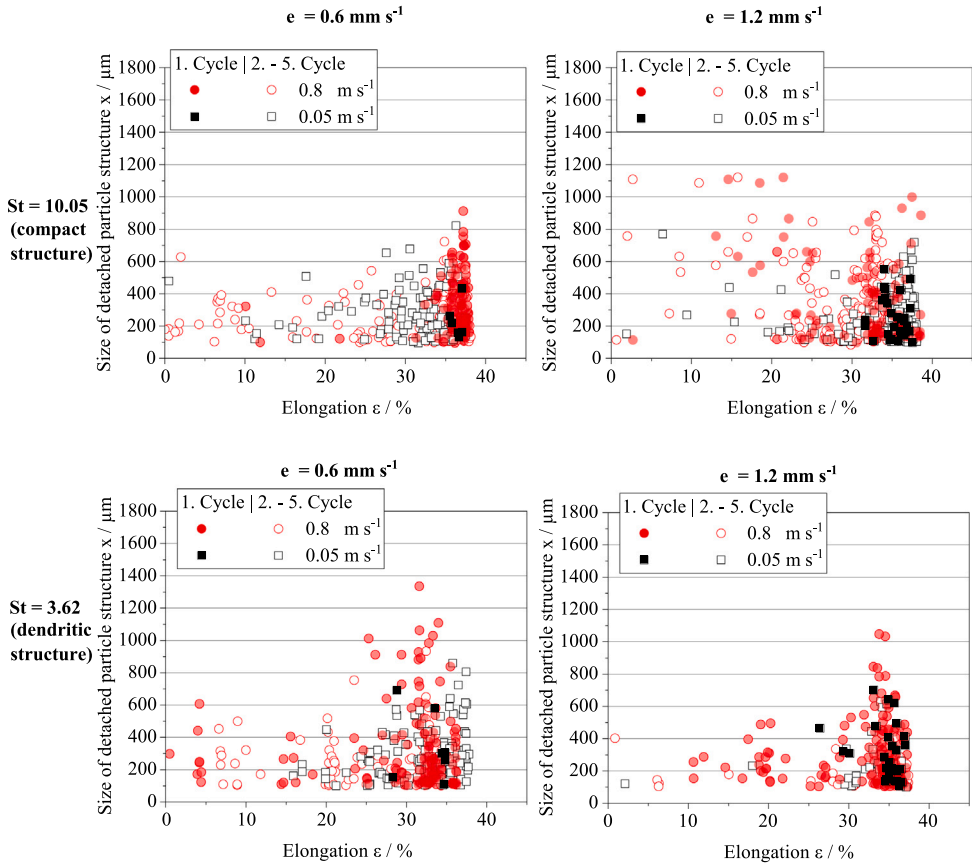

Fig. 9. Size of the detached particle structures as a function of the structural morphology (TOP: St = 10.05; BOTTOM: St = 3.62; Left: 0.6 mms^{-1}; Right: 1.2 mms^{-1}), as well as the elongation and flow velocity.

velocity can be kept constant at 0.05 m/s. In general, the effect of stretching velocity on the moment of detachment is less pronounced for dendritic (St = 3.62) structures than for compact (St = 10.05) structures.

3.3. Development of relative free projection area

Observation of the RFPI allows quantitative statements about the state of the interfiber spaces and pores after the stretching processes. The results presented here discuss the effects of flow velocity, stretching velocity, and initial morphology of the deposited particle structure. The data provides a more holistic view of the detachment process.

Fig. 10 shows the RFPI as a function of the number of stretching cycles for the compact structures at a Stokes number of 10.05 and 6.70, respectively. As a result of detachment of particle structure due to stretching, the RFPI increases with high air velocities of 0.8 m/s for all stretching velocities. The reached RFPI values after 5 stretching cycle are regardless of the morphology (St = 10.05; St = 6.70) of the initial structure.

An increase in stretching velocity also enhances the RFPI, except in the experiment with a particle structure generated at a Stokes number of 6.70 and an airflow velocity of 0.05 m/s during stretching. This single experiment show exactly the opposite. In general, an increase in the RFPI is always associated with a release of the interfiber spaces and a detachment of particle structures during the consecutive stretching cycle.

For the experiment with an airflow velocity of 0.05 m/s there are negative values in the first cycle for almost all experiment regardless the morphology (St = 10.05; St = 6.70) of the structure on the array. In these experiments the particle structure on the fiber move radial during stretching and remain within the fiber interspaces after relaxation (see Fig. 11, Left and Right). The drag force of the air flow and the break up of the particle structure by stretching are not sufficient to achieve detachment at the fiber distance of 246 µm. Nevertheless in the most cases, except the experiment(St = 10.05) and airflow velocity of 0.05 m/s, the RFPI value continues to increase as stretching cycles 2–5 progress. The bridges and agglomerates within the interspaces break during the following stretching cycle. In the case of the single exception, which is represented by the tests at St = 10.05 and an airflow velocity of 0.05 m/s, negative values of down to −54% are reached after a single stretching cycle (Fig. 10, Left). Further the RFPI decreases with each subsequent stretching cycle, reaching as low as −80% after 5 stretching cycle. In these experiments the particle structure on the fiber move radial during stretching and remain within the fiber interspaces after relaxation. (see Fig. 11, BOTTOM). The drag force of the air flow and the break up of the particle structure by stretching are not sufficient to achieve detachment at the fiber distance of 246 µm.

Since both compact and dendritic structures can occur in filtration processes using depth filters, it is important to investigate the detachment behavior of a dendritic initial structure from a fiber array during fiber stretching, in addition to the detachment behavior of compact structures. The initial structures formed under the corresponding flow conditions (St = 3.62 and St = 0.82) can be found in Section 3.1. Fig. 12 shows the corresponding values for the RFPI that have been reached during the five stretching cycles with simultaneous airflow. The RFPI increases in all cases, regardless of the initial dendritic structure (St = 3.62; St = 0.82), flow velocity, and strain rate, with an increasing number of strain cycles. The qualitative behavior is similar, although the slope varies.

For both initial structures (St = 3.62; St = 0.82), a significantly lower increase and a final value below 25% can be seen in the experiments with 0.05 m/s flow velocity. It can also be seen that the highest

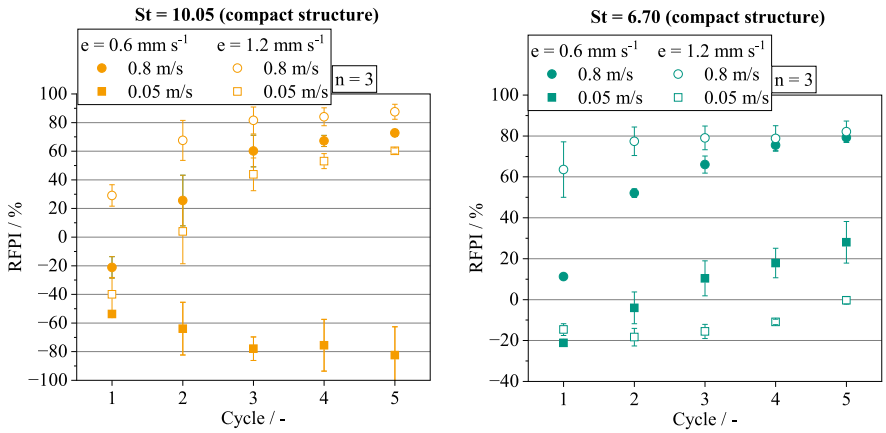

Fig. 10. RFPI of the stretching experiments with a compact particle structure on the fiber array.

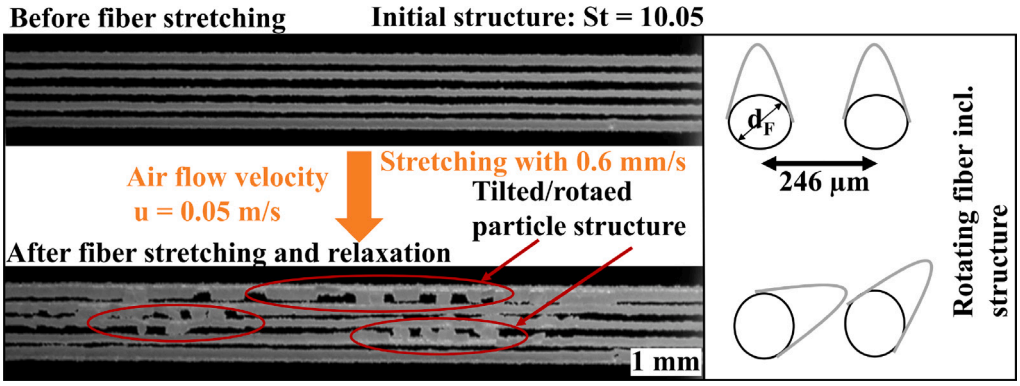

Fig. 11. Left: Image section of the fiber array before stretching and after the 2nd stretching cycle for compact structures with a Stokes number of 10.05. Right: Schematic representation of the tilting of the particle structures into the fiber interspaces during stretching. No reversal of the tilted particle structure after relaxation of the fiber.

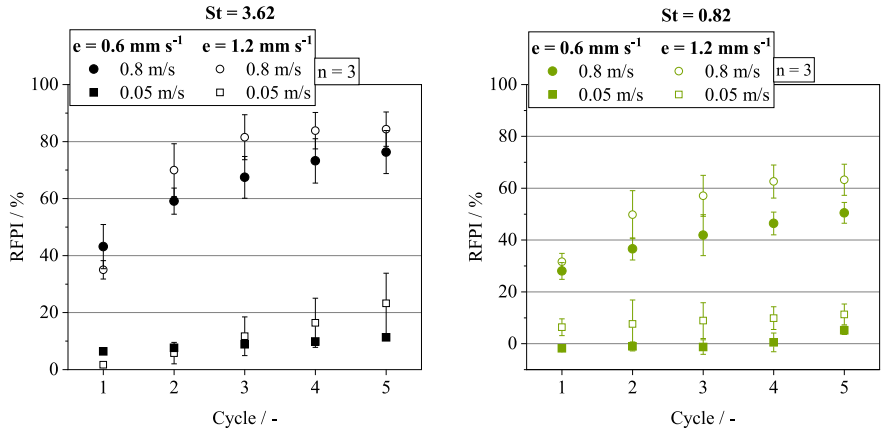

Fig. 12. RFPI plotted versus the number of stretching cycles for the investigated non-clogged dendritic particle structures (St = 3.62 and St = 0.82) on the fiber array for different air flow and stretching velocities.

final values for all experiments are obtained for the combination of a strain rate of 1.2 mm/s and a flow velocity of 0.8 m/s, regardless of the initial structure. The values of RFPI for the experiments with a strain rate of 0.6 mm/s are always lower than those with 1.2 mm/s, regardless of the initial structure and the incident flow velocity.

Further, there are no significant negative values of RFPI at the beginning of all experiments, which obtains that there is no rearrangement and rotation into the fiber interspaces of neighboring fibers during the stretching process as observed with the compact structure. Whether the particle structure remains on the fiber or the structure detaches during stretching.

In all experiments (St = 3.62; St = 0.82), regardless of the initial structure, it can be seen that increasing the flow velocity from 0.05 m/s to 0.8 m/s results in a significant increase of RFPI and also in the final values.

Overall lower final values of RFPI in the experiments with an initial structure deposited under deposition conditions of St = 0.82 (see Fig. 12, Right). For the experiments (St = 0.82) with an incident flow of 0.05 m/s there is very little increase and change in RFPI. The final value of RFPI is just under 5%. It is assumed that the higher porosity of the initial structure results from the ability of the structure to respond to the induced stress states by strain through rearrangement.

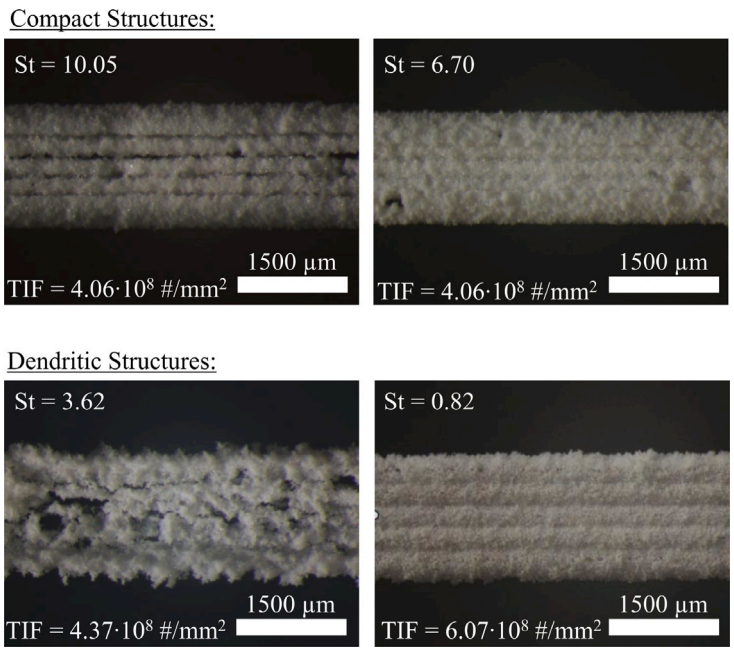

Fig. 13. Morphology of the clogged particle structures on the fiber array as a function of the Stokes number.

Observations of the moment of detachment of the particle structures and their size in the region of the initial dendritic structures on the array show the size of the particle structures and the moment of detachment during the stretching cycle (see Section 3.2.2).

3.4. Morphology and behavior of detachment of particulate structure on the fiber array after clogging

Fig. 13 shows macroscopic images of the clogged fiber arrays. The particle structures are deposited on the fiber array before the stretching process. The loading process is stopped individually for each morphology type after closure of gaps at the corresponding TIF given in Table 1.

The morphology of the clogged particle structures on the fiber array is a function of the Stokes number. Preliminary investigations on the development of the structures on the fiber array can be found in the studies of Poggemann et al. [8]. Compact and clogged structures (Fig. 13,TOP) are placed near to stagnation point of the fiber. The edges of the structure are mostly smooth and free of dendritic branches. If pores or gaps are still present, they tend to be elongated oriented parallel to the fiber interspaces. All structures on the individual fibers grow into the fiber interspaces with increasing TIF. The structures on the outer fibers grow faster and therefore close the outer spaces more than the inner ones. In particular, the particle structure revealed at a Stokes number of 10.05, the structures on the two outer fibers are very large and wide. Some breakouts can be seen within the formed structures (at St = 3.62). These could be caused by particles or agglomerates within the aerosol hitting the fiber with high kinetic energy due to their mass and airflow velocity.

The two lower images in Fig. 13 (BOTTOM) show the dendritic structures (St = 3.62; St = 0.82) before the stretching experiment. Compared to the compact structures, the dendritic branches are clearly visible in both regimes of the Stokes number.

The branches are more pronounced in the structure with a Stokes number of 3.62. It can also be seen that in this structure, due to the higher kinetic energy of the particles caused by the aerosol velocity, significantly more breakouts occur in these structures (at St = 3.62). Further the size of separated particles differs as they seem to be larger than for the structure at St = 0.82 (see Fig. 13, BOTTOM, RIGHT).

The structure formed at a Stokes number of 0.82, is completely clogged. Comparing the compact structure with the dendritic structure in the top view, it can also be seen that the dendritic structures grow much more into horizontal width starting from the fiber axis. zenith of the outer fibers than is the case with the compact structures.

3.5. Detachment of particle structures from a fiber array after clogging

3.5.1. General remarks on the behavior of clogged structures during stretching

In contrast to the non-clogged structures on the fiber at low TIF, clogged compact and dendritic structures exhibit significant differences in detachment behavior during stretching procedure. Nevertheless, three phases can again be distinguished here.

Phase 1 of the behavior of the particle structure starts with the fiber stretching. During the first phase of stretching, the behavior of the particle structure is independent of the morphology of the structure and is similar to non-clogged structures. The structure on the fiber moves slightly with the stretching of the underlying fiber and undergoes elongation without visible cracking within the deposited structure (in phase 1). This observation may be attributed to the fact that the structure on the fiber rests higher on the substrate, causing a delay in cracking from the surface of the particle structure to the fiber. Rearrangement, as observed in the compact and non-clogged particle structures on the fiber array, plays a minor role at high airflow velocities. In some cases, small pores or weak spots in the structure may start to crack during stretching and phase 1.

In the second phase, visible crack formation is observed for the compact structures with increasing stretching. These cracks emerge perpendicular to the direction of stretching throughout the entire particle structure extending over multiple neighboring fibers. In contrast to non-clogged structures, several cracks appear within the clogged particle structure on the fiber array.

Due to their increased porosity, dendritic structures do not exhibit cracking across the whole structure on the array. Instead, the cracks emerge locally in the area of a fiber or only locally.

In the third phase, particle structures start to detach from the array on the fiber. Dendritic and compact structures detach from the fiber array, leaving a residual structure on the array.

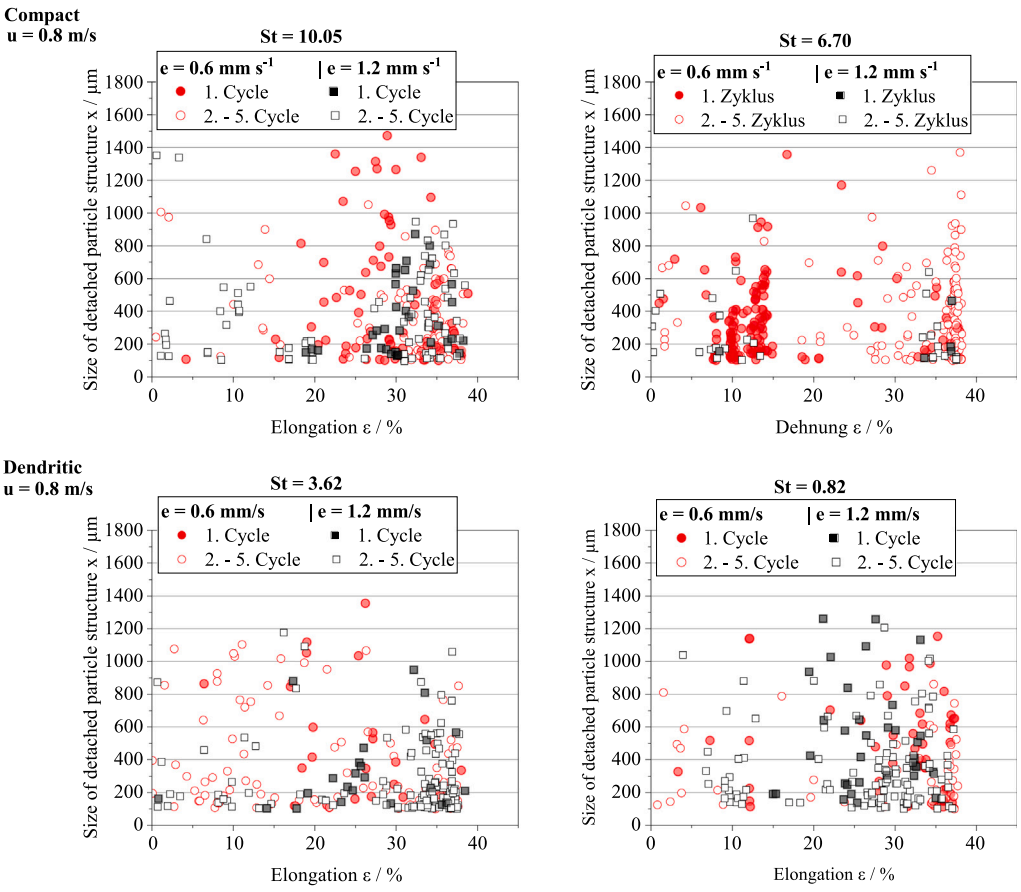

Fig. 14. Particle size as a function of structural morphology (BOTTOM: St = 3.62; TOP: St = 10.05), stretching velocity, and air flow velocity.

In all experiments with a clogged structure on the fiber array (TIF = 1.73 $\cdot 10^8$ #mm^{-2}) regardless of the morphology, no radial rearrangement was detected in the first stretching cycle. Radial rearrangement of structures occurred only when particle structures were already detached from adjacent fibers. The rearrangement process can then be based on the designs with an unclogged structure.

3.5.2. Moment of detachment of particle structures from an clogged fiber array

In addition to the experiments with a non-clogged structure on the fiber array, experiments were also carried out with a clogged particle structure on the fiber array.

The graph in Fig. 14 plot the size of the released particle structure over the fiber elongation at the moment of detection for each detachment event. Detachment events during the first cycle are represented by solid symbols, while events in the 2.-5. cycle are consolidated marked by outlined symbols. Air flow velocity remained constant at 0.8 m/s during all shown experiment in Fig. 14.

As with non-clogged structures, most particle agglomerates detach at high elongations between 25 to 38.50% stretching regardless of the structure morphology on the fiber. The majority of detached structures in the first stretching cycle are seen here. The particle structures in the second to fifth stretching cycles detach much earlier in the range of 0–20% fiber stretching, regardless of the morphology of the initial structure. The influence of the stretching velocity on the moment of detachment is negligible at the airflow velocity of 0.8 m/s as the influence of the airflow is expected to be predominant. This can be concluded from the previous observations on the single fiber but also on the array. However, in all cases a lower stretching velocity of 0.6 mm/s seems to favor the formation of larger detached structures.

Comparing the results to the experiments (u = 0.8 m/s, e = 0.6 mm/s) with a non-clogged structure, the detached structures in the experiment with a clogged structure have an average size of 350±28 µm, while the detached structures from a non-clogged structures had an average size of 265 ± 59 µm. In addition, compared to the detachment in the experiment with the non-clogged structures (see Section 3.2.2), there is a clear shift of the detachment area to lower fiber stretching (0–20%), which is also noticeable regardless of the morphology of the structure on the fiber. The detached structures also show a significant increase in size compared to the non-clogged structures. As clogged structures are stretched, more large particle agglomerates detach due to the increased particulate loading with the clogged array.

In experiments with a dendritic clogged initial structure (see Fig. 14, BOTTOM), fewer particle structures are detached in the first strain cycle than with a compact initial structure (see Fig. 14, TOP). This is probably due to the internal strength and porosity of the structures. Dendritic structures can better absorb initial stretching and rearrangement, as well as the introduction of stress, without loss of particle material. In addition, the detached particle structures are slightly smaller than those of the tests with a compact clogged initial structure. With respect to the different strain rates, there is also no difference between the 0.6 mm/s and 1.2 mm/s experiments.

In the all experiments with an air flow of 0.05 m/s, little or no detachment of the particle structures was observed, regardless of stretching velocity, as can be seen in the results of the RFPI in the following section. It can be assumed that although the clogged particle structure on the fiber array can be loosened by stretching the fiber, the drag force is reduced and sufficient to overcome the particle–particle or fiber-particle adhesion forces. More information on the lack of detachment in the experiments with a clogged particle structure on the array and an airflow velocity of 0.05 m/s can be found in Section 3.5.3.

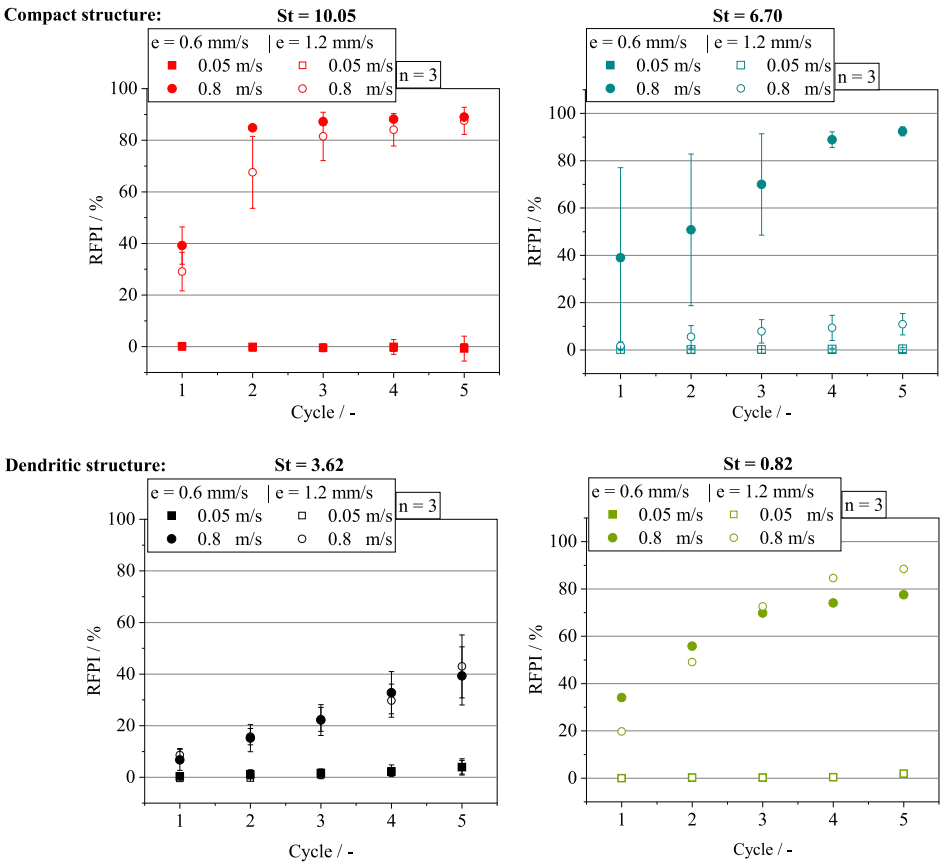

Fig. 15. RFPI after stretching procedure as a function of number of stretching cycles for the investigated clogged particle structures on the fiber array. Variation of air flow velocity, stretching velocities and morphology.

3.5.3. Development of RFPI for the clogged particle structure on the fiber array

Fig. 15 shows the variation of RFPI versus the number of stretching cycles of the clogged particle structures (Stokes number of 10.05; 6.70; 3.62 and 0.82), for two air flow velocities (0.05 and 0.8 m/s) with variation of the stretching velocities.

For all experiments with a low air flow velocity of 0.05 m/s, values of RFPI close to 0% are obtained for all morphology and stretching velocity. However, no detached particle structures were detected in these experiments (see Section 3.5.2). Clogged structures show improved stability compared to non-clogged particle structures on the fiber array. Due to the clogged structure, the particle-free air bypasses the fiber array during stretching instead of passing through fiber interspaces. As a result, no local flow channels are created in the fiber interspaces of the array. In a potential stretchable filter however, the air flow must pass through the filter, so detachment would be conceivable even at low air flow velocities. Further, The reason the drag force is not large enough, which may be due to the fact that the resistance caused by the flow is not large enough, or that the face area of the particle structure is not increased by radial rearrangement.

In the experiments with an increased airflow velocity of 0.8 m/s, large numbers of detached particle agglomerates were detected as shown in the results in Section 3.5.2. As a consequence, the RFPI increases as a function of stretching cycle for all experiments (St = 10.05; St = 6.70; St = 3.62; St = 0.82) regardless of the stretching velocity or the morphology of the particle structure on the fiber array.

Apart from the influence of the airflow velocity during stretching, the stretching velocity of the fiber has a small influence on the final value of RFPI. There are only small differences between the detected values of RFPI of the experiments with 0.6 mm/s or 1.2 mm/s. These are independent of the morphology of the structure.

3.6. Size of detached particle structures during stretching cycle

In the stretching experiment, the size of the particle structure's evolution over the five stretching cycles is crucial for the process, in addition to the process parameters and morphology. The size of particle structures determines whether the structures can be transferred into deeper layers of a filter or if they will remain suspended between or on the upstream fibers. This estimation is important for experiments involving both unclogged and clogged particle structures.

Fiber stretching initiates tensile and shear stress within the particle structure, leading to the introduction of cracks. Poggemann et al. demonstrated that large fragments detach from a single fiber due to dissolved cohesion during the first stretching cycle. In the subsequent elongation cycles, rather small residual structures are detached up to the empty fiber. In the tests involving compact structures on a single fiber, only the first stretching cycle and the second through fifth stretching cycles were analyzed [5].

Fig. 16 shows the mean size of the detached structures for two morphology types (St = 10.05 and St = 0.82; non-clogged and clogged structure) as a function of each stretching cycle. The results listed here were all determined in tests with an air flow velocity of 0.8 m/s. The results for the tests with an air velocity of 0.05 m/s can be found in SI, but do show a few time no significant values due to the lack of detachment of particle structures.

It can be seen that regardless of the particle structure present on the fiber array, the largest particle structures are detached from the fiber array in the first stretching cycle. As the number of stretching cycles increases, the size of the average detached particle structures in the stretching experiments with a stretching velocity of 0.6 mm s^{-1} decreases continuously from initially 500 to 150 µm. As confirmed in all experiments and the shown result in Sections 3.2.2 and 3.5.2, large

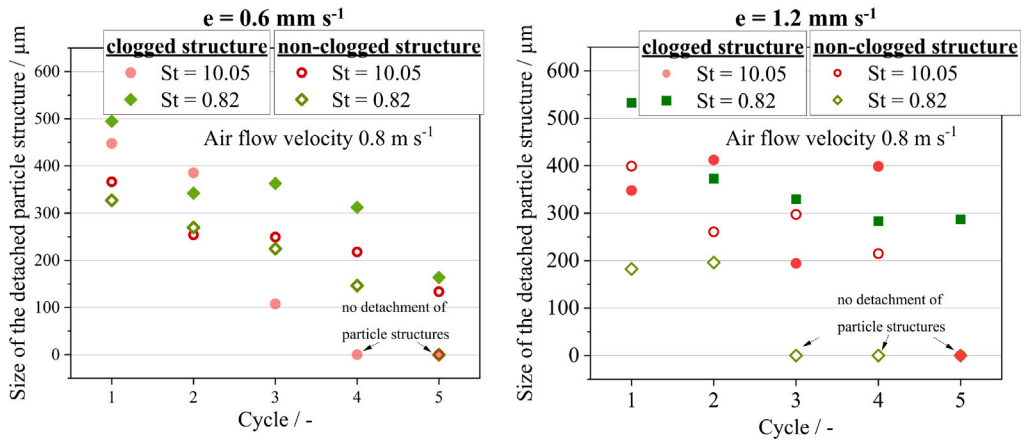

Fig. 16. Mean size of detached agglomerates from the fiber array as a function of each single stretching cycles for a compact and a dendritic initial structure. The stretching velocity is varied from 0.6 mm/s to 1.2 mm/s. Size values of 0 indicate "no detachment".

structures are detached from the fiber during the first cycle, similar to the description of the detachment process and observations. The bonds between particles, known as cohesion, dissolved first, so large structure detach. The isolated large structures between the cracks may be exposed to an increased flow force due to the airflow, as they offer a large face area. After the detachment of the large structures, a observed residual layer remains on the fiber. In the following stretching cycles, this residual layer detached regardless of its size. It is evident that the size of the detached structures in the clogged initial structure is generally larger than that of the non-clogged initial structure. This is due to the greater mass of particle material on the array, resulting in wider and taller particle structures.

However, the detached structures exhibit similar behavior to the compact structures, with a slight tendency towards larger structures in dendritic formations. This is likely due to the higher porosity of the agglomerates and the less compact structure of the fibers.

With increasing stretching velocity (see Fig. 16, right), the tendency of size of detached structures to decrease with increasing number of stretching cycles remains, but is not nearly as pronounced. Overall, the average size of the detached agglomerates, if any are detached at all in a single stretching cycle, is at a higher level. Whether particle material is still present on the fibers or not varies from case to case. In tests with dendritic initial structures, a residual structure of particle material tends to be present. For comparison, corresponding images can be found in the SI.

In the SI, mean particle size data for the lower airflow velocity of 0.05 m/s can be found. No significant trend towards decreasing or increasing size of the detached particles over the five stretching cycles was detected in this case.

3.7. Initiated multiaxial stress into particulate structure

The problem with uniaxial elongation and the tests performed on a clogged structure with an airflow velocity of 0.05 m/s is that it causes cracking to occur across the entire width of the array, transverse to the fibers, resulting in minimal detachment. The original idea behind conducting further tests based on the previous ones on the array is to induce cracking in diagonal arrangement (excluding a 90-degree angle to the fibers) in the area of the interfiber bridges. This aims to increase the shear stress in the deposited particle structure, leading to irregular breakage of the structure. The ultimate objective is to increase the likelihood of particle structure detachment. To increase the input of stress into the particle structure and especially to multiply the direction of the input as shown in Fig. 17, the preliminary experiments were performed with a fiber clamping device where the fiber distance can be increased or decreased by 27 µm during the stretching process (see Fig. 2 right hand). Fig. 18 shows the images of the particle structures before and after five stretching cycles to compare the change within the particle structure with and without a change in the fiber distance during the stretching processes. The compact and dendritic structures are depicted after the stretching processes with simultaneously reducing and increasing the fiber distance.

The left side of the figure shows the structure (compact and dendritic) without any change in fiber distance during stretching. Looking at the compact structure after five stretching cycles, the former cracks of a fractured structure can be seen in the circled enlargement. The images (refer to Fig. 18, LEFT TOP & BOTTOM) from the tests with compact and dendritic structures on the fiber show minimal differences before and after the stretching cycles. Although cracks form during elongation, they subsequently push together again during relaxation, resulting in a structure with internal weak points and irregular edges. Additionally, a few areas exhibit obvious detachment. For a first qualitative comparison of the influence of multiaxial stretching, the images of the experiments under the same test conditions before and after the stretching cycles (0.6 mm/s and 0.05 m/s; compact and dendritic structure), but with additional simultaneous change (reduction or extension) of the fiber distance, are shown in Fig. 18.

Looking at the images of the experiments with fiber distance reduction (see Fig. 18, MIDDLE), it is noticeable that the compact structures are slightly broken diagonally compared to the experiments without fiber distance reduction. However, the individual structures on the array are shifted and displaced much more by the multiple application of multidimensional stress. In addition, clear gaps can be seen as a result of particle structure detachment. Pores have also formed in the area of the inner fibers.

When comparing the tests with compact structure and expanded fiber distance (as shown in Fig. 18, RIGHT) to the tests with reduced fiber distance, the displacement and rearrangement are more pronounced. After 5 stretching cycles, the remaining large particle structures on the array are arranged diagonally on the fibers. It is evident that particle material has detached from the array. The increase in fiber distance, combined with stretching, leads to a more pronounced rearrangement of agglomerates, even if they are not directly detached from the array in the direction of flow. Some fibers also exhibit a residual structure. The breakup of the particle structures is similar to the breakup of a filter cake under shear stress and simultaneous dewatering/filtration.

The tests with a dendritic structure (see Fig. 18, MIDDLE & RIGHT BOTTTOM) on the array show a similar picture, although with a different fracture and rearrangement pattern. The structures are much more porous and do not form serious agglomerates during the five stretching cycles. In both the stretching experiment with distance reduction or

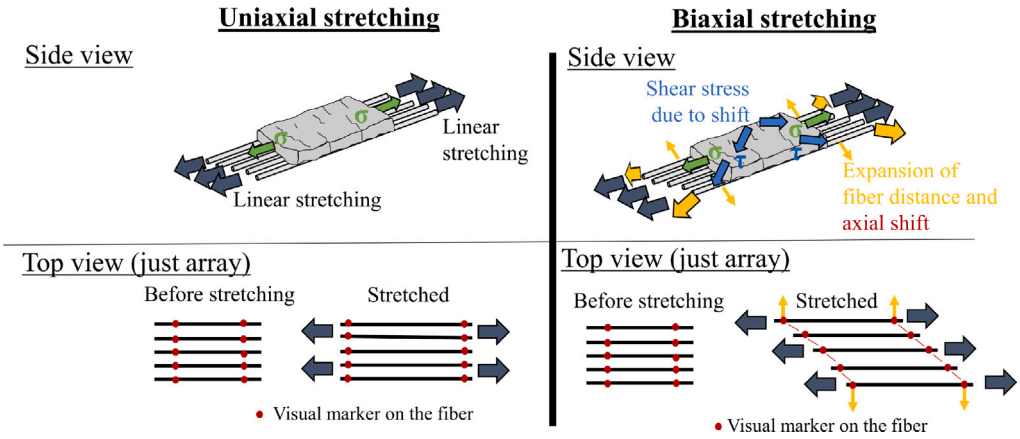

Fig. 17. Schematic on the differences between uniaxial and biaxial stretching in side and top view. The stretching and displacement of the fibers are indicated by visual markers in the case of biaxial elongation.

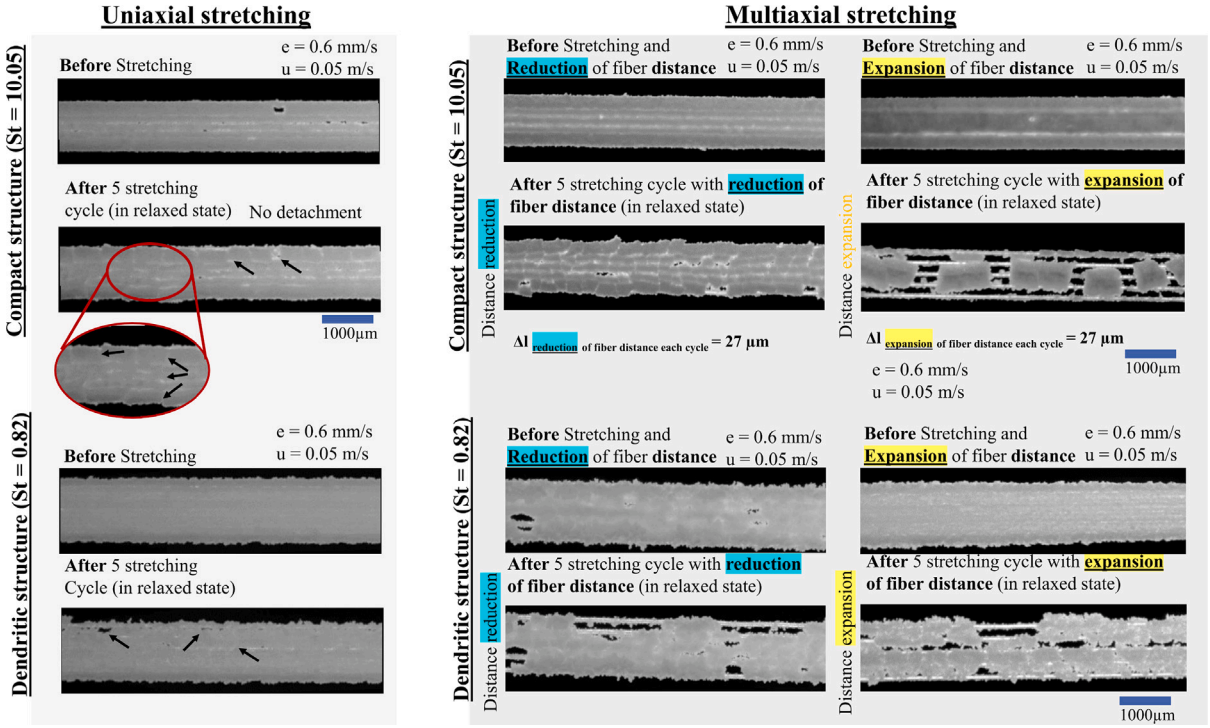

Fig. 18. Compact and dendritic particle structure before and after five elongation cycle without and with change of fiber distance during the elongation process.

expansion, the structures are irregularly fractured. Applied stress has different effects on porous structures compared to compact structures due to clearly defined crack formation, as previously described by Thouless [20,23].

4. Conclusion

In this study, the influence of stretching and simultaneous particle-free flow on the rearrangement and detachment of particle agglomerates from an deposited structure (dendritic or compact) on an array (5 fibers) was investigated. The particle structures consist of inert glass material and were deposited on the fiber via a filtration process. The evaluation of the rearrangement process during the stretching of the underlying fiber array was based on a quantitative analysis of the unblocked area in the fiber interspaces and the size of the detached particle structures. In addition, a qualitative analysis was performed to examine the fracture pattern and the different phases of the fracture and detachment process. The main results are:

- Identification of three phases during fiber stretching and detachment of particle structures independent of the morphology of the initial structure on the fiber array, but not on time integrated flux (TIF).
- The radial rearrangement of the particle structures of a non-clogged initial structure led to unexpected clogging of the fiber interspaces at low inflow and elongation velocities.
- As already observed in the single fiber experiments, an increase of the inflow velocity leads to a premature detachment time of the particle structures.
- Significant increase in the final relative free projection area of fiber interspaces (RFPI) after 5 stretching cycles when the velocity of the particle-free inflow is increased from 0.05 m/s to 0.8 m/s, regardless of the presence of TIF.
- The size of the detached particle structures decreases with increasing number of stretching cycles — independent of the morphology of the initial structure and partly also of the loading condition (non-clogged and clogged).

- The moment of detachment occurs prematurely with increasing stretching velocities.
- In preliminary tests it was found that in addition to the uniaxial elongation of the fiber array, the simultaneous change of the fiber distance (reduction or expansion of 27 μm) increases on the break-up and detachment of particle structures.

5. Outlook

As the results show, the expectation that the multiaxial stress introduction leads to an increased detachment of the particle structures from the collector is well justified in the preliminary experiments. However, the experiments on an array with a clogged particle structure have revealed new challenges of radial rearrangement and the blocking of fiber interspaces by rotating particle structures during fiber elongation and low air flow velocities.

Investigations of the rearrangement in the depth of the filter would be conceivable using a stacked multi-row arrangement of fibers as an array. This arrangement of fibers (in an array) would make it possible to study what happens to the first detached particulate material as it moves through the fiber arrangement in the direction of flow within a filter.

It might be also conceivable to perform a discrete element method (DEM) simulation like Braschke et al. on an array with stretchable fiber to get an idea of the stress within the particle structure under multidimensional stretching situation [33]. First tests on a stretchable single fiber have already been performed in a DEM simulation environment.

In addition to these more fundamental aspects, the next step would be to look at the macro level of the experiment — on entire stretchable filter. The detachment of particle structures by stretching the filter matrix is a task for future investigations. In addition to the specific knowledge of detached or penetrated particulate material, it would then be possible to find the relationship between the rearrangement of particulate material and a potential change in pressure drop. Different cleaning strategies and the influence of the multidimensional stress state could be initiated and experimentally tested with a three-dimensional filter matrix.

6. Abbreviations

DEM	discrete element method
MFC	mass flow controller
LSDS	Large Structure Detection System
RFPI	relative free projection area of fiber interspaces
SI	Support Information
TIF	time integrated flux

CRediT authorship contribution statement

Lukas Poggemann: Writing – original draft, Visualization, Validation, Software, Project administration, Methodology, Investigation, Formal analysis, Data curation, Conceptualization. **Pablo Längle:** Visualization, Methodology, Investigation, Data curation. **Jörg Meyer:** Writing – review & editing, Formal analysis, Conceptualization. **Achim Dittler:** Writing – review & editing, Supervision, Funding acquisition, Conceptualization.

Declaration of competing interest

The authors declare that they have no known competing financial interests or personal relationships that could have appeared to influence the work reported in this paper.

Data availability

Data will be made available on request.

Declaration of Generative AI and AI-assisted technologies in the writing process

During the preparation of this work the authors used DeepL in order to integrate figures and to examine sections of the manuscript for spelling and grammar. After using this tool, the authors reviewed and edited the content as needed and take full responsibility for the content of the publication.

Acknowledgments

We kindly thank Freudenberg Filtration Technologies SE & Co. KG for donating fiber material. We gratefully acknowledge that this project was funded by the Deutsche Forschungsgemeinschaft (DFG, German Research Foundation) - 427981860.

I would like to thank Marco Hummel and the mechanical workshop at MVM for their assistance in the design and manufacture of the parts produced.

Appendix A. Supplementary data

Supplementary data associated with this article can be found, in the online version, at https://doi.org/10.1016/j.seppur.2024.127887

References

[1] K. Hoppe, M. Maricanov, G. Schaldach, R. Zielke, D. Renschen, W. Tillmann, M. Thommes, D. Pieloth, Modeling the separation performance of depth filter considering tomographic data, Environ. Progress Sustain. Energy (2020) http://dx.doi.org/10.1002/ep.13423.

[2] K. Hoppe, L. Wischemann, G. Schaldach, R. Zielke, W. Tillmann, M. Thommes, D. Pieloth, Filtration kinetics of depth filters—Modeling and comparison with tomographic data of particle depositions, Atmosphere 14 (4) (2023) 640.

[3] D. Thomas, P. Penicot, P. Contal, D. Leclerc, J. Vendel, Clogging of fibrous filters by solid aerosol particles experimental and modelling study, Chem. Eng. Sci. (56) (2001) 3549–3561.

[4] L. Poggemann, J. Meyer, A. Dittler, A novel method to investigate detachment of particulate structures from an elastic single fiber at low gas flow velocities, J. Aerosol Sci. 156 (2021) 105785, http://dx.doi.org/10.1016/j.jaerosci.2021.105785.

[5] L. Poggemann, J. Meyer, A. Dittler, Experimental detection of particle structures detachment from a stretchable single fiber during multiple consecutive stretching cycles, Separations 9 (7) (2022) 168, http://dx.doi.org/10.3390/separations9070168.

[6] J. Szabadi, J. Meyer, A. Dittler, In situ characterization of particle structures generated at different flow velocities on a single fiber in the gas phase, J. Aerosol Sci. 173 (2023) 106197.

[7] J. Zoller, Abscheidung reaktiver und inerter Partikeln aus Aerosolen auf einzelnen Fasern und Ablösung der entstandenen Strukturen durch Umströmung bei gleichzeitiger Reaktion (Ph.D. thesis), Karlsruher Institut für Technologie (KIT), 2023, http://dx.doi.org/10.5445/IR/1000165523.

[8] L. Poggemann, R. Thelen, J. Meyer, A. Dittler, Experimental investigation on the change of pull-off force between bulk particulate material and an elastic polymeric filter fiber, J. Colloid Interface Sci. 641 (2023) 903–915.

[9] T. Müller, Trägheitsabscheidung von partikeln an parallelen faserarrays, in: Verfahrenstechnik, Dr. Hut, München, 2017.

[10] M. Siena, M. Riva, J. Hyman, C. Winter, A. Guadagnini, Relationship between pore size and velocity probability distributions in stochastically generated porous media, Phys. Rev.. E, Stat., Nonlinear, Soft Matter Phys. 89 (1) (2014) 013018.

[11] K. Alim, S. Parsa, D.A. Weitz, M.P. Brenner, Local pore size correlations determine flow distributions in porous media, Phys. Rev. Lett. 119 (2017) 144501, http://dx.doi.org/10.1103/PhysRevLett.119.144501.

[12] I. Griffiths, I. Mitevski, I. Vujkovac, M. Illingworth, P. Stewart, The role of tortuosity in filtration efficiency: A general network model for filtration, J. Membr. Sci. 598 (2020) 117664.

[13] Y. Song, E. Shim, Structure characterization of the clogging process of coarse fibrous filter media during solid particle loading with X-ray micro-computed tomography, Sep. Purif. Technol. 273 (2021) 118980, http://dx.doi.org/10.1016/j.seppur.2021.118980.

[14] Y. Song, E. Shim, 3D X-ray tomographic microstructure analysis of dust-clogging inside nonwoven fibrous filter media, J. Membr. Sci. 664 (2022) 121067, http://dx.doi.org/10.1016/j.memsci.2022.121067.

[15] Y. Song, E. Shim, High-fidelity 3D simulation of dust-loading behavior and clogging process of coarse nonwoven filter media considering collision effect, Sep. Purif. Technol. 344 (2024) 127046, http://dx.doi.org/10.1016/j.seppur.2024.127046.
[16] K. Shi, G. Jin, W. Yan, H. Xing, Permeability estimation for deformable porous media with convolutional neural network, Internat. J. Numer. Methods Heat Fluid Flow (2024).
[17] T. Müller, J. Meyer, G. Kasper, Low Reynolds number drag and particle collision efficiency of a cylindrical fiber within a parallel array, J. Aerosol Sci. 77 (2014) 50–66, http://dx.doi.org/10.1016/j.jaerosci.2014.07.007.
[18] L. Poggemann, B. King, J. Meyer, A. Dittler, Morphology ofdin2012779 particulate structures on a fiber array before and at clogging point of an aerosol filtration process, Separations 10 (9) (2023) 462.
[19] J. Zoller, A. Zargaran, K. Braschke, J. Meyer, U. Janoske, A. Dittler, Morphology of particulate deposits formed on a single filter fibre by exposure to mixed aerosol flow, J. Aerosol Sci. (2020) 105718, http://dx.doi.org/10.1016/j.jaerosci.2020.105718.
[20] J.L. Beuth, Cracking of thin bonded films in residual tension, Int. J. Solids Struct. 29 (13) (1992) 1657–1675, http://dx.doi.org/10.1016/0020-7683(92)90015-L.
[21] R. Nahta, B. Moran, Crack spacing in brittle films on dissimilar planar and axisymmetric elastic substrates, Eng. Fract. Mech. (52) (1995) 513–524.
[22] R. Nahta, B. Moran, Film cracking and debonding in a coated fiber, Int. J. Fracture (79) (1996) 351–372.
[23] M.D. Thouless, Crack spacing in brittle films on elastic substrates, J. Am. Ceram. Soc. (73) (1990) 2144–2146.
[24] C. Jia, Z. Wang, D. Zhang, T. Zhang, X. Meng, Fracture of films caused by uniaxial tensions: A numerical model, Appl. Math. Mech. 44 (12) (2023) 2093–2108, http://dx.doi.org/10.1007/s10483-023-3061-7.
[25] S. Ochiai, Y. Murakami, Theoretical prediction of tensile strength of fibers as a function of thickness of brittle zones on fiber surfaces, Metall. Trans. A (12A) (1981) 1155–1161.
[26] Q. Wang, X. Lin, D.-R. Chen, Effect of dust loading rate on the loading characteristics of high efficiency filter media, Powder Technol. 287 (2016) 20–28, http://dx.doi.org/10.1016/j.powtec.2015.09.032.
[27] V. Papapostolou, H. Zhang, B.J. Feenstra, A. Polidori, Development of an environmental chamber for evaluating the performance of low-cost air quality sensors under controlled conditions, Atmos. Environ. 171 (2017) 82–90, http://dx.doi.org/10.1016/j.atmosenv.2017.10.003.
[28] J. Raasch, H. Umhauer, Grundsätzliche überlegungen zur messung der verteilungen von partikelgröße und partikelgeschwindigkeit disperser phasen in strömungen, Chem. Ing. Tech. 49 (12) (1977) 931–941, http://dx.doi.org/10.1002/cite.330491203.
[29] S. Wurster, J. Meyer, G. Kasper, On the relationship of drop entrainment with bubble formation rates in oil mist filters, Sep. Purif. Technol. 179 (2017) 542–549, http://dx.doi.org/10.1016/j.seppur.2017.02.036.
[30] D. Kampa, S. Wurster, J. Buzengeiger, J. Meyer, G. Kasper, Pressure drop and liquid transport through coalescence filter media used for oil mist filtration, Int. J. Multiph. Flow 58 (2014) 313–324, http://dx.doi.org/10.1016/j.ijmultiphaseflow.2013.10.007.
[31] J. Zoller, A. Zargaran, K. Braschke, J. Meyer, U. Janoske, A. Dittler, A novel apparatus for simultaneous laser-light-sheet optical particle counting and video recording in the same measurement chamber at high temperature, Sensors 22 (4) (2022) 1363, http://dx.doi.org/10.3390/s22041363.
[32] J. Szabadi, J. Meyer, A. Dittler, Particulate matter detachment from a magnetizable single fiber applying magnetic forces in ambient air, Separations 10 (5) (2023) http://dx.doi.org/10.3390/separations10050297.
[33] K. Braschke, J. Zoller, A. Zargaran, A. Dittler, U. Janoske, Analytical and numerical calculation of the detachment of particle structures from fibers, Aerosol Sci. Technol. 56 (1) (2022) 1–11, http://dx.doi.org/10.1080/02786826.2021.1972085.